Carbon storage and immobilization in a large scale aquifer - Guarani Aquifer System

K. Miotliński[1], L. Peeters[2]

[1]Universidade Federal de Santa Catarina, Departamento de Engenharia Sanitária e Ambiental

[2]CSIRO Land and Water

[1]Campus Universitário Trindade, Florianópolis SC 88040970, Brazil

[2]Private Bag 2, Glen Osmond SA 5064, Australia

Key Points:

- Reactive transport modeling (RTM) shows that natural recharge of CO_2-rich water into an aquifer with aluminosilicate minerals is capable of providing negative carbon feedback, although its efficiency declines with higher fluxes.
- The CO_2 flux, plagioclase and olivine hydrolysis rates play an important role in dissolved solute concentrations and carbon storage, while ion exchange delays its effect.
- Soil pH, horizontal hydraulic conductivity, porosity, secondary mineral precipitation reactions, but calcite precipitation and Mg^{2+} ratio in precipitating carbonates play a minor role in carbon feedback on this scale.

Corresponding author: Konrad Miotliński, konrad.miotlinski@gmail.com

Abstract

Giant aquifers are capable of storing significant amounts of carbon as a result of immense water volumes, substantial dissolved inorganic carbon (DIC) concentrations and its ubiquitous reactions with matrix, thus contributing the global carbon storage and cycle. However, concentrations of dissolved solutes vary significantly over a distance in the Guarani Aquifer System (GAS) which causes difficulties in process interpretation. To quantify the importance of controlling parameters, we performed reactive transport modeling which combines both hydrological and geochemical inputs. The paper presents a chemical evolution in a two-dimensional aquifer configuration, global sensitivity analysis along with estimates of the DIC flux through the system boundaries. We observed that the DIC flux at recharge as well as plagioclase and olivine hydrolysis rates play an overriding importance in controlling the solute patterns including the DIC concentrations, while soil pH, horizontal hydraulic conductivity, porosity, precipitation of secondary minerals, but calcite, and Mg^{2+} ratio in carbonates are of minor significance. If released Ca^{2+} undergoes ion exchange to Na^{+}, the storage is delayed in time and space. In conclusion, the capacity of GAS in receiving recharge CO_2 is attributed to the hydrolysis along with advective transport while the global sensitivity analysis informs how the financial resources should be allocated to effectively reduce interpretative uncertainty in large-scale groundwater systems.

1 Introduction

The subsurface is an important inorganic carbon reservoir and groundwater is gaining attention as to which extent it contributes to the global carbon cycle. Estimates of carbon fluxes in the subsurface are hugely uncertain due to difficulties in (1) calculating groundwater and chemical fluxes (Fontaine et al., 2007; McCallum et al., 2012; Y. Li et al., 2015), (2) subsurface conceptualization (Enemark et al., 2019; Vilhelmsen et al., 2018a), and (3) parametrization (Vilhelmsen et al., 2018b) as well as (4) the dynamic role of soils in CO_2 storage and its downward leakage (Kessler & Harvey, 2001; Fontaine et al., 2007; Sánchez-Cañete et al., 2018).

In-situ measurements of a CO_2 and O_2 couple in soils indicate that significant amounts of CO_2 produced in a shallow subsurface does not, at least immediately, return to the atmosphere due to (1) dissolution in groundwater, (2) transport in gaseous or dissolved forms, (3) mineral weathering (Sánchez-Cañete et al., 2018). Consequently, the CO_2 dis-

solution coupled with advective transport may lead to significant amounts of dissolved inorganic carbon (DIC) stored in groundwater bodies (Y. Li et al., 2015; Zhang & Planavsky, 2020) that may be transported over long distances, undergo geochemical transformations and, finally, be discharged to rivers (Gaillardet et al., 1999) or sea (Zhang & Planavsky, 2020).

Thus, when CO_2 passes through the soil profile the geochemical transformations depend on reactivity of aquifer material. The carbonate and silicate minerals participate in the transformation process (Zhong et al., 2017; Oelkers et al., 2018; Pogge von Strandmann et al., 2019). The DIC reaction with aluminosilicate minerals, which is referred as chemical rock weathering (CRW) may be associated with precipitation of secondary minerals resulting in a long-term carbon storage (Berner, 1998; Steffen et al., 2007; Maher & Chamberlain, 2014; Oelkers et al., 2018). Nevertheless, the reaction pathways are complex and heterogeneous and may depend on a variety of factors including: (1) groundwater flow velocity (Maher & Chamberlain, 2014), (2) thermodynamic equilibria and dissolved ion availability (Zhang & Planavsky, 2020) or (3) rates of dissolution and precipitation (Pogge von Strandmann et al., 2019).

Reactive transport models (RTM) may be useful in interpretation and quantification of the transformation patterns. The use of RTMs can be justified by a need to incorporate a coupling between the chemical processes with groundwater flow and solute transport (Steefel et al., 2005), to integrate various kinds of data into a single model (Bethke et al., 2002; Jessen et al., 2017; Jakobsen et al., 2018) or to perform a global sensitivity analysis to investigate the importance of controlling parameters (Dai et al., 2014). Depending on an objective of modeling, RTMs may include groundwater flow/soil water infiltration rate, dispersive mixing and solute diffusion. These capabilities make RTMs suitable in studying process understanding and quantification of geochemical fluxes (Bethke et al., 2002; Jessen et al., 2017; L. Li et al., 2017; Bao et al., 2017; Jakobsen et al., 2018).

Although a deep groundwater drainage pathway is integrated into the evaluation of global rates, there is a little knowledge on how much carbon is stored in large aquifers, how much may get naturally immobilized through secondary precipitation and what parameters govern the carbon cycle. To estimate the carbon fluxes in the one of the world's most voluminous Guarani Aquifer System (GAS), we developed a coupled RTM in which we integrate physical properties of the aquifer with the geochemical reactions. We per-

formed global sensitivity analysis to identify the importance of individual parameters and we verified our model by comparing its results with the groundwater quality data observed along the flow paths.

2 Site description and methodology

2.1 Hydrogeology of the aquifer

The Guarani Aquifer System (GAS) is one of the most voluminous groundwater bodies on the Earth due to its great geographical extend and a large thickness (Foster et al., 2009). The study focuses on the NE part from where we compiled hydrogeological and geochemical information (Araujo et al., 1999; Gastmans et al., 2010; Hirata et al., 2011). In this region, the system is a part of the Paraná Basin which consists of stratified sandstone series of Triassic (Piramboia unit) and Cretaceous (Botucatu unit) ages. The formation is up to 832 meters thick, with the average thickness of 400 meters (Araujo et al., 1999). Reported hydraulic conductivity and porosity values are in the range 0.0864 - 0.864 m/d (Rebouças, 1994; De Paula E Silva & Cavaguti, 1994) and 0.16-0.24 (Rebouças, 1976; Hirata et al., 2011), respectively.

About 10% of the formation outcrops, whereas the remaining part is confined by a sequence of basalts of the Serra Geral formation (Fernandes et al., 2016). The GAS is underlain by siltstones containing highly mineralized groundwater of the Passa Dois Group (Silva, 1983; Meng & Maynard, 2001).

Natural aquifer recharge of GAS dominates as direct percolation of precipitation through the outcrop areas. The deep groundwater recharge estimated with the water level fluctuation method accounts locally for up to 50 mm/year, which is 3.5% of the mean annual precipitation (Wendland et al., 2007). No estimates have been performed for the confined part of the aquifer, but since the basalt formation is intersected with dikes (Fernandes et al., 2016) and groundwater samples contain ^{14}C (Aggarwal et al., 2015), infiltration of recent rainwater through the overlying basalt unit seems to be taking place. Downstream, in the deeply confined part of the aquifer, elevated Cl^- concentrations along with crust ^4He gas dissolved in groundwater suggest recharge from the underlying formations (Aggarwal et al., 2015). The groundwater flow is radially diverging and the discharge takes place in the Paraná River valley, where artesian conditions are apparent (Rebouças, 1994).

Groundwater residence times evaluated using the ^{81}Kr isotope vary in the broad range of 80 to 820 ky (Aggarwal et al., 2015). This indicates that the average linear groundwater velocities are from 0.15 to 1.25 m/year and, consequently, that GAS has been flushed at least 180 times since its deposition which was followed by a number of tectonic events with the most recent one between 88 and 65 million years ago (Araujo et al., 1999).

2.2 Hydrogeochemical evolution

The chemical composition of groundwater exhibits a zonation from fresh Ca-HCO_3 and Ca-Mg-HCO_3 water types in unconfined/marginal parts of the basin towards brackish Na-HCO_3-Cl and Na-Cl in the central part (Fig. 1 and Gastmans et al. (2010)). The evolution has been suggested to be a result of either aluminosilicate weathering (Silva, 1983; Gastmans et al., 2010) or cation exchange coupled to carbonate dissolution (Sracek & Hirata, 2002). The mineral matrix, however, is composed of chalcedony near the outcrop and calcite cement in the deep confining zone (Hirata et al., 2011). There is evidence of aluminosilicate transformation including dissolution of plagioclase and K-feldspar as well as formation kaolinite and smectites (Hirata et al., 2011). Labradorite is a dominant plagioclase, while both orthoclase and microcline represent K-feldspar (Gesicki, 2007).

The underlying sediments contain highly mineralized groundwater with Total Dissolved Solids (TDS) of up to 2,000 mg/L and H_2S in some boreholes (Hirata et al., 2011). The deep groundwater from Águas de São Pedro (22 ^{o} 35 $'$ 30 $"$ S, 47 ^{o} 53 $'$ 38 $"$ W) contains $Na^+ = Cl^-$ 29 mM (Soler i Gil & Bonotto, 2014). Highly mineralized waters may result in the increase in TDS from a few to 700 mg/L, $\delta^{13}C_{DIC}$ from -19 to -5 and from 4.7 to 9.5 per mille, respectively, in a depth profile (Appendix A1).

The $\delta^{13}C_{DIC}$ and pH are typical of a closed siliciclastic system in which the former is driven by dissociation of carbonic acid and the latter by the proton reaction with the aquifer material (Clark, 2015). The initial pH of 4.7 and low alkalinity (5 mg/L) suggest that if soil CO_2 is the only source of acidity in the infiltrating water, the dissolved inorganic carbon (DIC) concentrations may be as high as 3 mM with the corresponding log pCO_2 of -1.7 (Appelo & Postma, 2005).

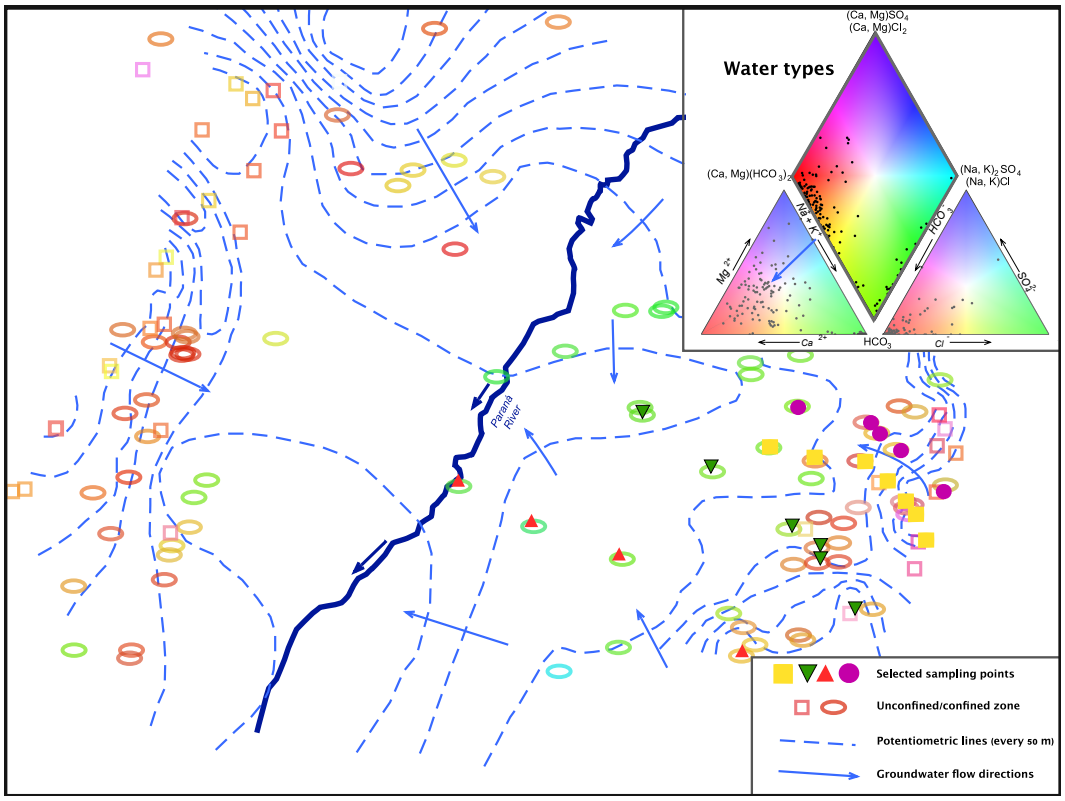

Figure 1. Groundwater sampling locations in confined (ellipses) and unconfined (squares) parts of the aquifer. Hue indicates types as from the Piper diagram diamond. The Paraná river flows across the region from the NE to SW

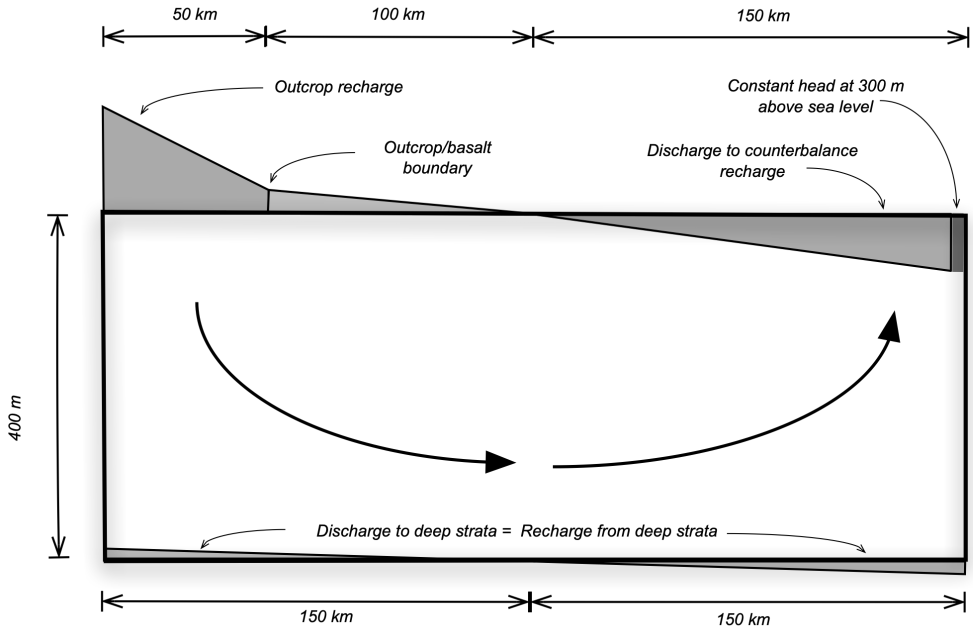

Figure 2. Conceptual 2D model of the water flow in the GAS with shaded polygons depicting water fluxes through the boundaries. The upper boundary is divided into three sections: (1) 50 km outcrop, (2) 100 km recharge from basalt, (3) 150 km discharge to basalt

2.3 Conceptual and numerical models

We conceptualized a groundwater system as a two-dimensional (2D) vertical cross-section parallel to the direction of groundwater flow (Freeze & Witherspoon, 1968). The system is a rectangular with the dimensions 300 km and 400 m in length and thickness, respectively (Fig. 2). We imposed groundwater flow field by using the flux boundary condition along the upper and lower boundaries of the system.

The USGS PHAST code (Parkhurst et al., 2010) with PHREEQC database was used to simulate reactive transport in the 2D domain (Fig. 2). The domain was divided into 31 and 401 nodes in a vertical and horizontal direction, respectively, which correspond to the depth and distance. In addition to flux boundary conditions at the upper boundary (Fig. 2), we assigned a single node at 300 km with a constant boundary con-

dition to assure a numerical stability of the solution. The model is run 1 million years to assure the system reaches steady-state.

Chemical fluxes through the system are products of water flux and concentrations. The recharge water at the outcrop contains only CO_2 (log pCO_2 = -1.7, i.e. soil pH = 4.6 and C = 3mM), which is meant to react with the aquifer material. We consider the basalt recharge as either CO_2 water or groundwater equilibrated with log pCO_2 = -1.7, plagioclase, olivine and chalcedony. This is to explore whether groundwater recharge with high concentrations of Ca^{2+}, Mg^{2+}, and SiO_2 through basalts is capable of changing the water quality patterns in the GAS itself. The basement water is highly-mineralized Na-Cl groundwater of the Passa Dois Group (Meng & Maynard, 2001; Soler i Gil & Bonotto, 2014) which recharges the GAS (Hirata et al., 2011; Aggarwal et al., 2015) (Tab. 1).

We selected a number of geochemical reactions to be held in the aquifer that are consistent with the conceptual understanding of silicate groundwater system and were capable of controlling the observed concentrations. Firstly, we developed a simple model of plagioclase ($Ca_{0.5}Na_{0.5}Al_{1.5}Si_{2.5}O_8$) hydrolysis coupled with chalcedony (SiO_2), kaolinite ($Al_2Si_2O_5(OH)_4$) and calcite ($CaCO_3$) precipitation as well as ion exchange to demonstrate 2D and profile average concentrations. Secondly, we included olivine (Mg_2SiO_4) and K-feldspar ($KAlSi_3O_8$) dissolution coupled with K-mica ($KAl_3Si_3O_{10}(OH)_2$) and illite ($K_{0.6}Mg_{0.25}Al_{2.3}Si_{3.5}O_{10}(OH)_2$) precipitation to include Mg^{2+} and K^+ in the analysis as well as Mg^{2+} incorporation in the calcite 1. Thus, the weathering reactions were kinetically controlled with the 0th order reaction rates. We justified the choice of the reaction order by a strong subsaturation of the minerals. The secondary reactions are equilibrium controlled (Postma & Jakobsen, 1996).

The effect of ion exchange was studied in the simpler model and we used cation exchange capacity (CEC) 2.5 mM/L with Na^+ initially filling the sorption sites. The value of CEC corresponds to values encountered in other siliciclastic aquifers (Appelo, 1994; Appelo & Postma, 2005; Walraevens et al., 2007).

An ensemble of 1000 parameter combinations was generated with Latin Hypercube Sampling (Tab. 1) and evaluated with the RTM to carry out a global sensitivity analysis. We used the delta moment-independent measure technique developed by Borgonovo (2007); Plischke et al. (2013), as implemented in the SALib python library (Herman & Usher, 2017). The technique calculates a total sensitivity index value between a param-

Table 1. Parametrization of the reactive transport models with ranges explored in global sensitivity analysis

	Simple	Complex		
		$\bar{X}$	σ	*Comment*/distribution
Max rech. rate (outcrop)	0.0025	0.0017	0.0012	Log-normal
Outcrop rech. quality	C = 3 mM	C = 3 mM	-	Fixed
Max rech. rate - basalt	0.0003	0.001	0.0008	Log-normal
Basalt rech. quality	C = 3 mM	C = 3 mM	$Calcite + Kao + Chal$	*equilibrium*
Basement rech. quality	5 mM NaCl	19 mM NaCl	-	$DeepGW$[a]
Kx	0.33 m/d	0.33 m/d	0.1m/d	Log-normal
Kz	0.033 m/d	0.17 m/d	0.1 m/d	$f(recharge)$
Porosity	0.22	0.22	0.1	Normal
Soil pH	4.6	5.5	0.5	Normal
log $R_{Plagioclase}$	-16.05	-16.3	0.8	Normal
log $R_{K-feldspar}$	-	-17.2	0.8	Normal
log $R_{Olivine}$	-	-17.0	0.8	Normal
log $K_{Calcite}$	-8.48	-8.48	0.25	Normal
SI_{Illite}	-	0	0.25	Normal
SI_{K-mica}	-	0	1.0	Normal
Mg ratio for Calcite	-	0.17	0.1	Uniform
Cation exchange cap.	2.5 mM/L	-	-	-
Average GW vel.	0.56 m/yr	0.61 m/yr	0.48 m/yr	$f(recharge)$

[a] Águas de São Pedro (Soler i Gil & Bonotto, 2014)

eter of the model and a model output. Higher values indicate that the model outcome is more sensitive to parameter values.

To compare the modeling results with the field data (Gastmans et al., 2010) we selected a number of monitoring wells that are located along interpreted flow paths and we calculated distances from the basin's margin (Tab. C1).

3 Results and discussion

3.1 Controls of plagioclase hydrolysis in a 2D siliciclastic system

Our results show that in a 2D aquifer receiving a CO_2 solution, plagioclase hydrolysis is capable of developing distinct peaks of Ca^{2+} and total alkalinity ($HCO_3^- + CO_3^{2-} + H_3SiO4^- + H_2SiO4^{2-}$) as well as a gradual increase in pH (Fig. 3a, c and e). Average concentrations in a profile is a simplified depiction of the patterns, which allows one to compare with the observed GAS values.

Plagioclase hydrolysis drives the stoichiometric increases in Ca^{2+} and Na^+ and the intensity of the process depends on the chemical rate. Initially, the process directly consumes CO_2 and protons producing silicic acid and carbonate alkalinity (Equation 1):

$$\begin{aligned} &2Ca_{0.5}Na_{0.5}Al_{1.5}Si_{2.5}O_8 + CO_2 + 6.5H_2O + 2H^+ \rightarrow \\ &1.5Al_2Si_2O_5(OH)_4 + 2H_4SiO_4^0 + Na^+ + Ca^{2+} + HCO_3^- \end{aligned} \tag{1}$$

Once groundwater becomes saturated with respect to chalcedony, its precipitation takes place which prevents a continuous increase of SiO_2 in the solution (Equation 2):

$$\begin{aligned} &2Ca_{0.5}Na_{0.5}Al_{1.5}Si_{2.5}O_8 + CO_2 + 2.5H_2O + H^+ \rightarrow \\ &1.5Al_2Si_2O_5(OH)_4 + 2SiO_2 + Na^+ + Ca^{2+} + HCO_3^- \end{aligned} \tag{2}$$

Next, at a pH $\approx$ 7 groundwater becomes saturated with respect to calcite. At this pH value, the HCO_3^- is a dominant carbonate species which is being consumed, consequently, leading to calcite precipitation (Equation 3):

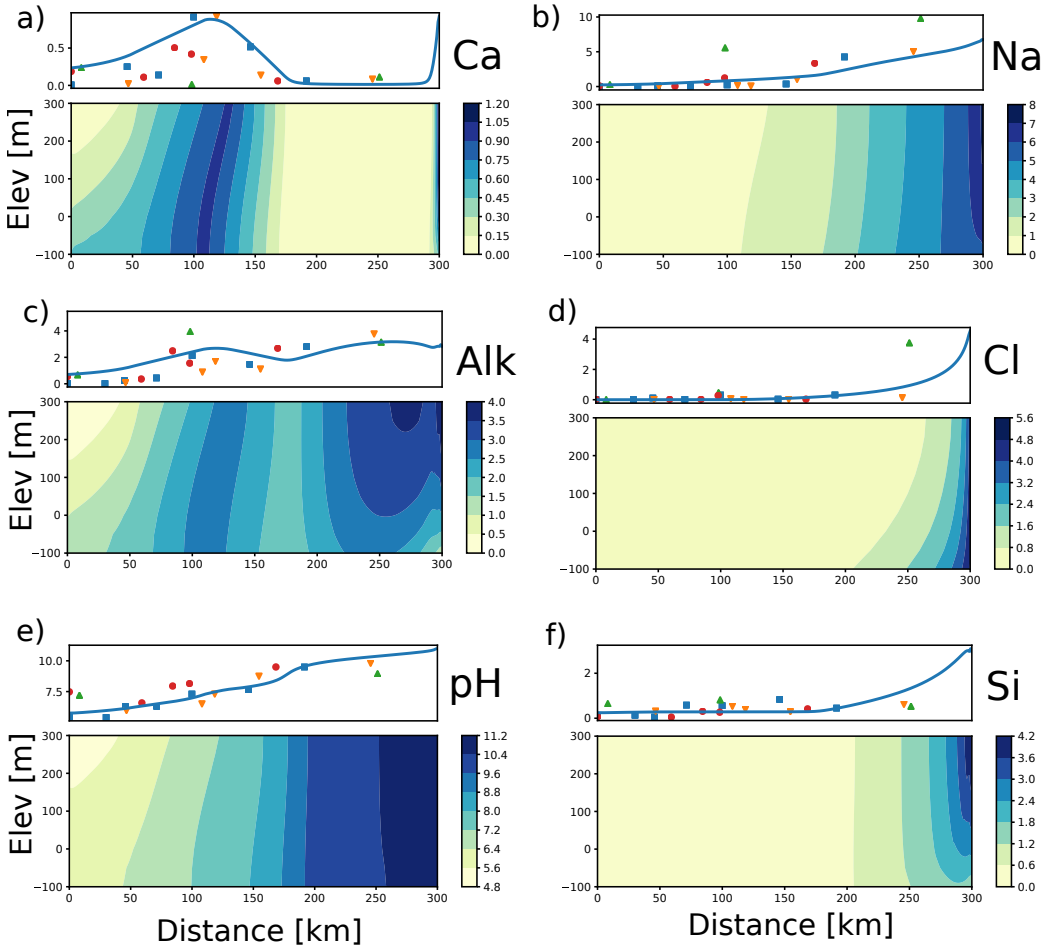

Figure 3. Profile average (measured and modelled) and 2D distribution of concentrations (mM) and pH due to plagioclase hydrolysis and associated secondary reactions

$$2Ca_{0.5}Na_{0.5}Al_{1.5}Si_{2.5}O_8 + HCO_3^- + 2.5H_2O + H^+ \rightarrow$$
$$1.5Al_2Si_2O_5(OH)_4 + 2SiO_2 + Na^+ + CaCO_3 \quad (3)$$

The increase in pH causes carbonic acid to dissociate (Fig. 4a) and once groundwater becomes saturated with calcite, precipitation takes place (Fig. 4b). Mass balance indicates that 50% of carbon is being immobilized as $CaCO_3$ and this is reflected by saturation index (Appelo & Postma, 2005) for calcite (Fig. 4c).

Plagioclase continues on being dissolved at higher pH values producing the dissociated $H_3SiO_4^-$ (Equation 4):

$$2Ca_{0.5}Na_{0.5}Al_{1.5}Si_{2.5}O_8 + HCO_3^- + 5.5H_2O + H^+ \rightarrow$$
$$1.5Al_2Si_2O_5(OH)_4 + 2H_3SiO_4^- + Na^+ + CaCO_3 \quad (4)$$

Production of $H_3SiO_4^-$ (Equation 4) causes an increase in the total Si concentration (Fig. 3f).

Ion exchange, which replaces Ca^{2+} for Na^+ in a solution, tends to smooth out the reactions fronts, leading to a more subtle Ca^{2+} peak and, subsequent i.e. from 150 km downstream, the absence of Ca^{2+} as well as increases in alkalinity and Na^+.

Nevertheless, the Na^+ and Cl^- concentrations from 150 to 300 km are chiefly a result of the inflow from the underlying strata as the boundary concentations are 5 mM. Since the bottom recharge Na:Cl ratio is 1, any number larger than 1 is a result of plagioclase hydrolysis and ion exchange.

3.2 Sensitivity of the model output to selected parameters

Multiple runs of the complex model (Tab. 1) show that hydraulic head distribution is the most sensitive output. The output depends on flux through boundaries rather than horizontal hydraulic conductivity (Fig. 5). Chemical flux, which is a product of recharge and DIC concentration at inflowing boundaries, strongly affects pH (decline) and DIC concentration (increase). This means that if DIC concentration at inflow is high, the relative DIC removal is low.

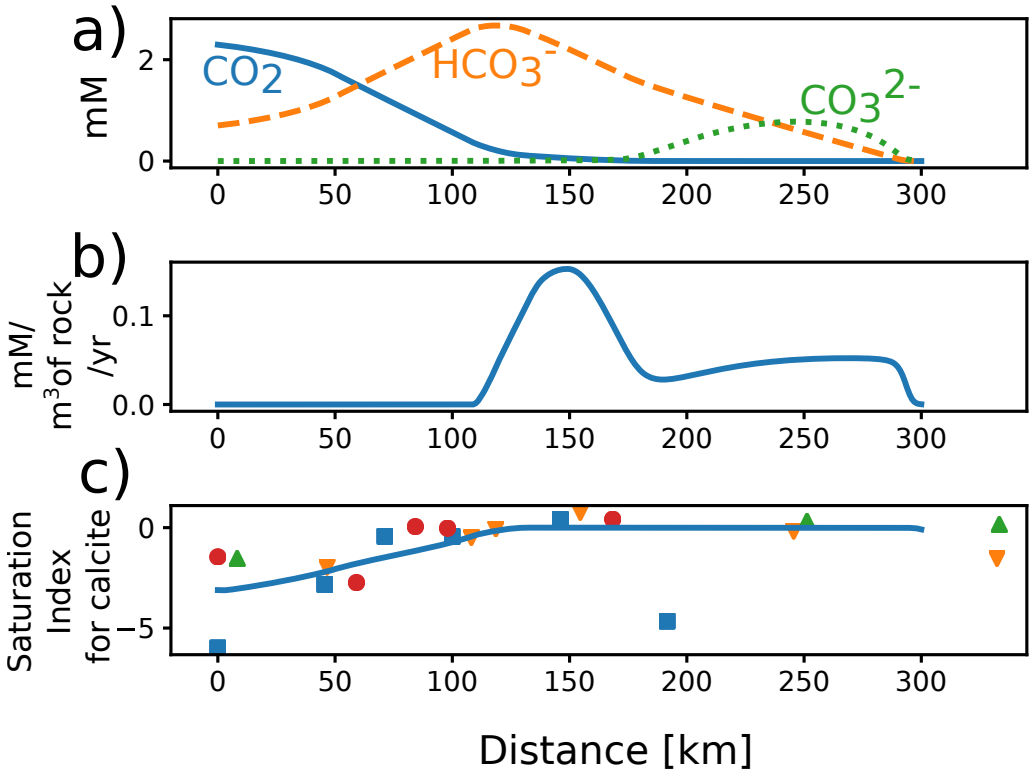

Figure 4. Concentrations of (a) dissolved carbonate species and (b) precipitated calcite and (c) measured (points) and calculated (line) saturation index for calcite in a function of distance

From among the chemical variables pH and DIC concentrations are the most sensitive outputs, followed by SiO_2, alkalinity and Ca^{2+}.

Plagioclase hydrolysis rate seems to be the most important parameter for several outputs (pH, Ca^{2+}, alkalinity, Na^+ and SiO_2). High rates result in augmenting pH and diminishing DIC. Moreover the said parameter affects Ca^{2+}, Na^+ and SiO_2 concentrations that are directly derived from this mineral. The elevated rate of olivine dissolution results in high Mg^{2+} concentration and pH and lower DIC concentration, with a negligible effect on alkalinity.

The DIC concentrations are dominated by chemical flux rates, plagioclase and olivine rates, but are not much influenced by stability of secondary minerals. Low sensitivity for calcite is somehow surprising and suggests that the complex model may be overconstrained.

Both secondary geochemical reactions and soil pH do not seem to play a significant role in solute concentrations. Although pH of infiltration water is very important in the small scale studies (Hansen & Postma, 1995; White & Brantley, 2003), its effect disappears on a larger scale.

Due to low influence of carbonate precipitation on DIC, Ca^{2+}, and pH, the Mg^{2+} ratio incorporated in freshly precipitated $CaCO_3$ does not significantly affects the results.

Similar outputs at distances 50, 150 and 250 km from the edge of the model indicate that it does not really matter which part of the aquifer we sample groundwater to identify the most influential parameters. Nevertheless, importance of weathering parameters keeps on increasing over the distance, as the concentrations derived from mineral hydrolysis increase too.

3.3 Distribution of carbon flux through the boundaries

The Upper Recharge Boundary is a principal source of carbon in the system (Tab. 2 and Fig. 6, for the simple and complex models, respectively). In both models the highest flux occurs in the outcrop area which is related with highest flux of recharge water in combination with DIC concentrations. The Upper Discharge Boundary also receives significant C fluxes and in the complex model they are concentrated near the edge of the model domain (Fig. 6).

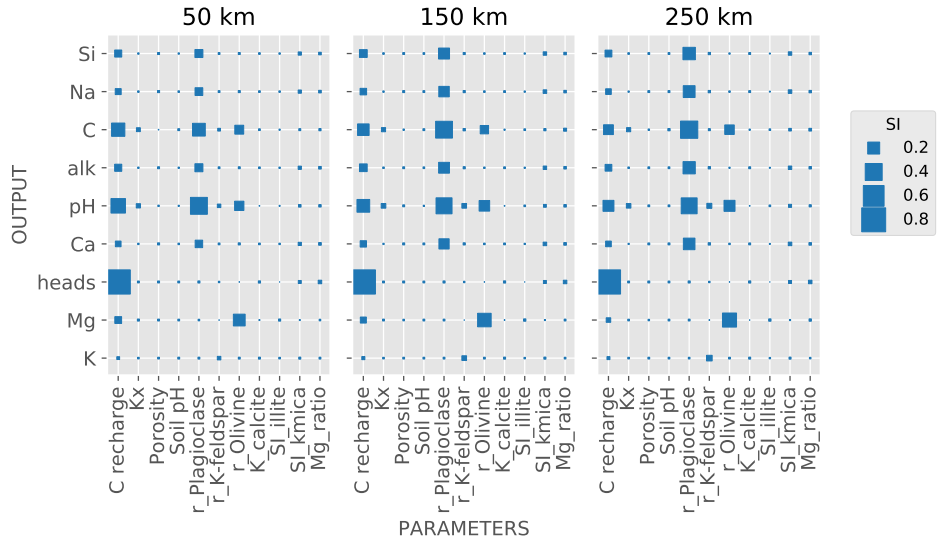

Figure 5. Results of global sensitivity analysis for different distances from the model edge. The values are given in Appendix B

The simple model indicates that 50% of DIC is effectively removed in the aquifer. If the GAS area is 1,195,500 km^2, this corresponds to 4.08×10^{11} M/yr or 4.9×10^6 T/yr.

Table 2. Water and carbon balance in the simple model

Boundary		water flux [mm/year]	C flux [M/m^2/year]
Upper	left	2.42	7.266×10^{-3}
	outcrop	6.33	1.9×10^{-2}
	basalt	0.45	1.346×10^{-3}
Lower	left	-0.43	-1.300×10^{-3}
Upper	right	-2.42	-2.991×10^{-3}
Lower	right	0.43	0
Imbalance		0	-2.975×10^{-3}

The lower boundaries participate in carbon fluxes too. Nevertheless, very few DIC is exchanged through the lower boundary due to low recharge rates and concentrations.

The Upper Discharge Boundary offers a sink for DIC. Although the fluxes are high (Fig. 6) due to water discharge rates, the total C outflux from the aquifer is smaller than

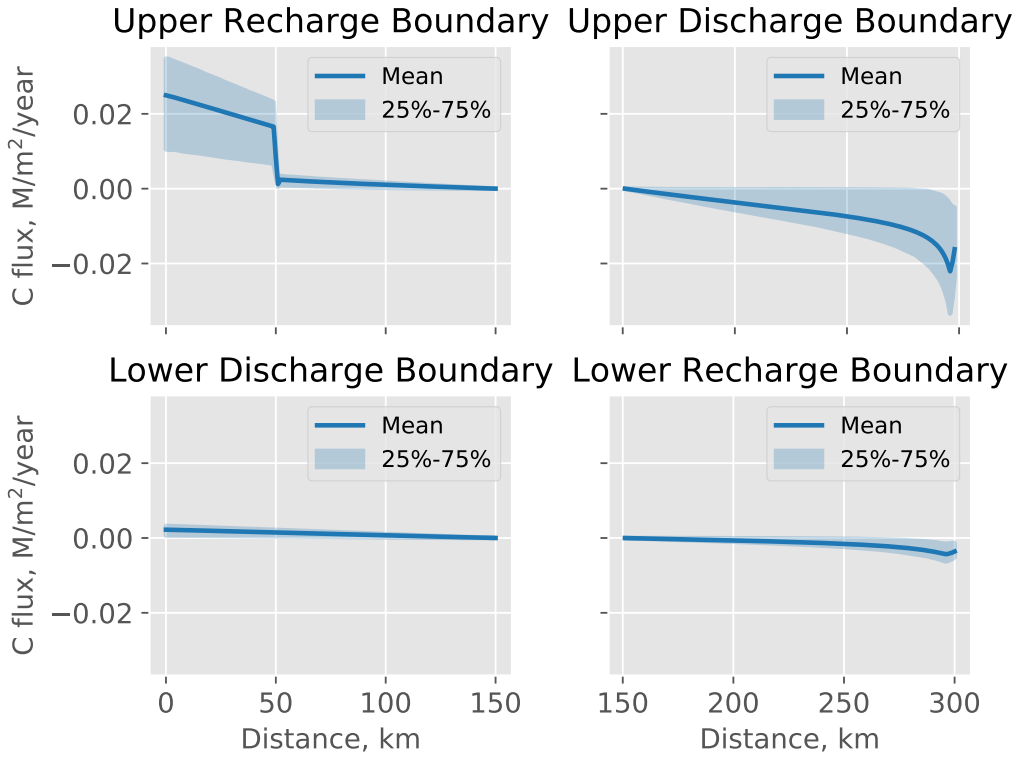

Figure 6. Carbon flux through the boundaries of the modelled system for 1000 model realisations. Positive values indicate downward direction and negative values indicate upward direction

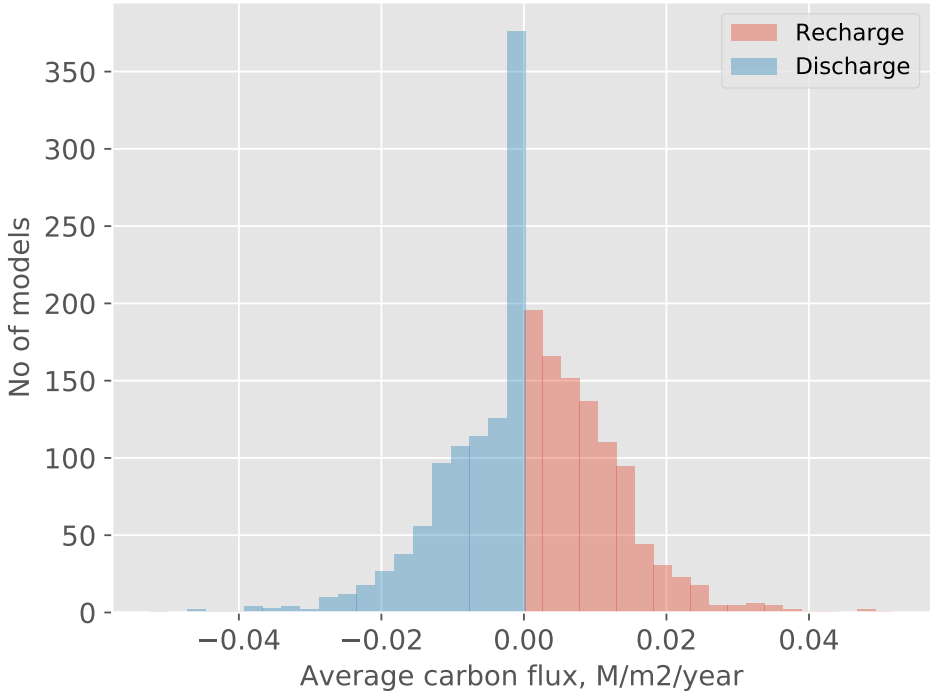

Figure 7. Histograms of carbon flux at recharge and discharge

the total influx (Tab. 2 and Fig. 7). The imbalance is a result of carbon accumulation and precipitation in the aquifer.

3.4 Improvements to the conceptual model

The numerical modelling suggests that a significant amount of carbonate may precipitate in a plagioclase system recharged with CO_2-rich groundwater. Authigenic carbonates are consistent with the field observations (Gesicki, 2007; Hirata et al., 2011) and inconsistent with the suggestions of carbonate removal coupled with ion exchange as a result of groundwater freshening (Sracek & Hirata, 2002). If ion exchange is an important process, our modelling implies that Na^+ is a dominant cation in the sorption sites.

We hipothesize that diffusion from the underlying strata has been occuring since the formation of the aquifer (Aggarwal et al., 2015), which could have caused the replacement of Ca^{2+} and Mg^{2+} with Na^+ in the sites.

An assumption of the constant recharge and carbon infiltration rates is motivated with a relatively small cyclical variations of climate in Brazil over the years (Cruz et al., 2005; Rodríguez-Zorro et al., 2020).

Recharge of Mg-rich water from the basalts does not seem to be capable of replacing the residing solution in the GAS to the extent of significantly modifying the water quality. However, locally, the process may be of importance. This would require dominance of advective flux from the basalts in relation to the outcrope along with contrasts in water quality.

The numerical model with its all simplifications underpins the importance of depth specific rather than depth integrated groundwater sampling for process identification (Appelo & Postma, 2005). Even in a relatively simple chemical configuration of an aquifer composed of plagioclase solely receiving CO_2 with a constant 0th order dissolution rate, the concentration patterns show unexpected complexity both laterally and vertically. The effect is exacerbated by low flow rates in the aquifer.

When the modeled mean groundwater velocities are compared with water residence times derived from ^{81}Kr data, it is clear that the simulations cover the range of the observed values (Fig. 8). Nevertheless, there are observation points that show much slower flow velocity than the mean value from all models. In those points the concentrations derived from weathering (Ca^{2+}, Mg^{2+}, Alkalinity) are likely to be higher than average due to longer residence times.

4 Conclusions

Natural recharge of CO_2-rich water into an aquifer with aluminosilicate minerals is capable of providing negative carbon feedback.

Reactive transport modeling can be used to integrate groundwater flow with a complex suite of geochemical reactions taking place in a siliceous aquifer which receives dissolved inorganic carbon (DIC) with recharge water. A simple conceptualization with a plagioclase mineral only suggests that 50% of carbon is immobilized as $CaCO_3$. By using global sensivitity analysis with a more complex model, we confirmed that the DIC fluxes and weathering rates of aluminosilicate minerals have a major significance in controlling solute concentrations and, consequently, DIC outflux at the discharge zone. Surprisingly, other parameters including horizontal hydraulic conductivity, soil pH, poros-

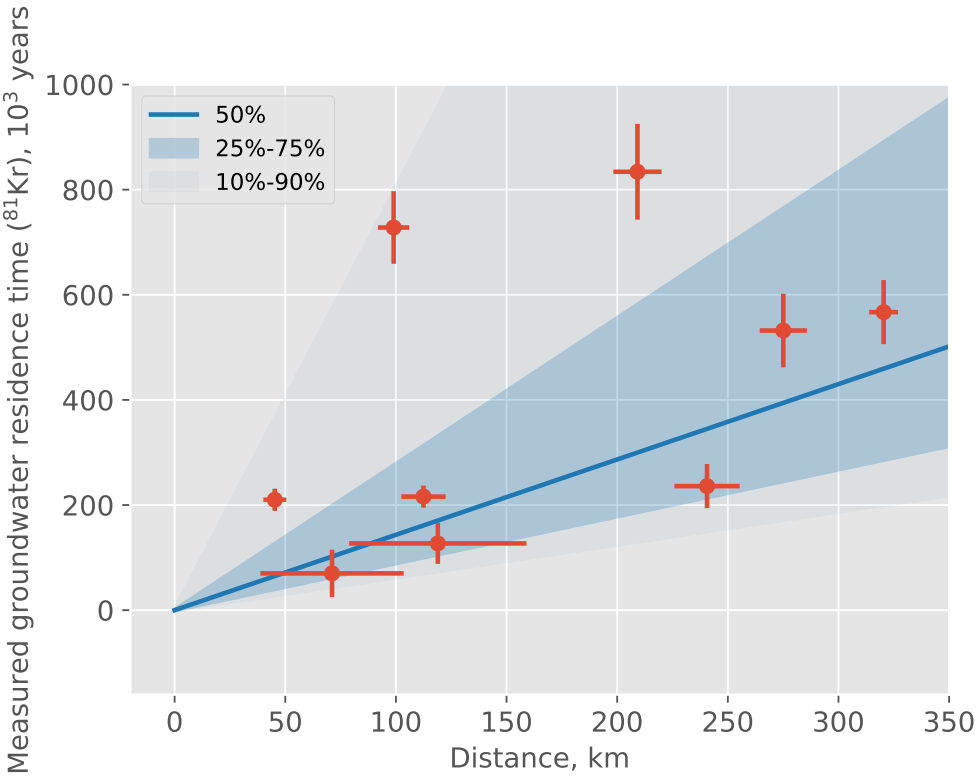

Figure 8. Groundwater residence times as a function of distance from basin margin derived from the isotopes (red points with uncertainty ranges, Aggarwal et al. (2015)) and groundwater model realizations (blue lines)

ity and stability of secondary minerals but Calcite play a minor or negligible role in controlling solute concentrations.

We anticipate that reactive transport models, combined with global sensitivity techniques, lead to improvements in understanding of the reactive patterns and reduce error of model predictions.

In order to better understand the role of large aquifers like GAS, the effort should be placed on:

- estimation of recharge rates using variety of methods and their integration,
- evaluation of DIC concentration in recharge water (Kessler & Harvey, 2001; Sánchez-Cañete et al., 2018),
- incorporation of Ca^{2+} and Mg^{2+} isotopes to understand the weathering rates and pathways of DIC cycling in the subsurface (Pogge von Strandmann et al., 2019).
- distribution of CEC in the aquifer and composition of the sorption sites.

Acknowledgments

Prof. Dieke Postma (GEUS, Denmark) is acknowledged for friendly and very useful remarks on the previous version of the manuscript. Numerous discussions with Dr. Elias Terramoto and Prof. Hung Kung Chang from UNESP, Rio Claro helped to develop the conceptual model of Guarani Aquifer System. The numerical model repository is located on *https://www.hydroshare.org/resource/b0c0815fbc4949ad9d0c21102df93a39/*. Measured concentraions from GAS are from (Gastmans et al., 2010) and from the deeper formation at Águas de São Pedro from (Soler i Gil & Bonotto, 2014).

References

Aggarwal, P. K., Matsumoto, T., Sturchio, N. C., Chang, H. K., Gastmans, D., Araguas-Araguas, L. J., ... Torgersen, T. (2015). Continental degassing of 4He by surficial discharge of deep groundwater. *Nature Geoscience*, *8*(1), 35–39. doi: 10.1038/ngeo2302

Appelo, C. A. J. (1994). Cation and proton exchange , pH variations , and carbonate reactions in a freshening aquifer. *Water Resources*, *30*(10), 2793–2805.

Appelo, C. A. J., & Postma, D. (2005). *Geochemistry, Groundwater and Pol-*

lution, Second Edition. Taylor & Francis. Retrieved from https://www.taylorfrancis.com/books/9781439833544 doi: 10.1201/9781439833544

Araujo, L. M., Franca, A. B., & Potter, P. E. (1999). Hydrogeology of the Mercosul aquifer system in the Paraná and Chaco-Paraná Basins, South America, and comparison with the Navajo-Nugget aquifer system, USA. *Hydrogeology Journal*, *7*, 317–336.

Bao, C., Li, L., Shi, Y., & Duffy, C. (2017, mar). Understanding watershed hydrogeochemistry: 1. Development of RT-Flux-PIHM. *Water Resources Research*, *53*(3), 2328–2345. Retrieved from http://doi.wiley.com/10.1002/2016WR018934 doi: 10.1002/2016WR018934

Berner, R. A. (1998). The carbon cycle and CO2 over Phanerozoic time: The role of land plants. *Philosophical Transactions of the Royal Society B: Biological Sciences*, *353*(1365), 75–82. doi: 10.1098/rstb.1998.0192

Bethke, C. M., Zhao, X., & Torgersen, T. (2002). Groundwater flow and the 4 He distribution in the Great Artesian Basin of Australia . *Journal of Geophysical Research: Solid Earth*, *104*(B6), 12999–13011. doi: 10.1029/1999jb900085

Borgonovo, E. (2007). A new uncertainty importance measure. *Reliability Engineering and System Safety*, *92*(6), 771–784. doi: 10.1016/j.ress.2006.04.015

Clark, I. (2015). *Groundwater Geochemistry and Isotopes*. CRC Press. Retrieved from https://www.taylorfrancis.com/books/9781466591745 doi: 10.1201/b18347

Cruz, F. W., Burns, S. J., Karmann, I., Sharp, W. D., Vuille, M., Cardoso, A. O., ... Viana, O. (2005, mar). Insolation-driven changes in atmospheric circulation over the past 116,000 years in subtropical Brazil. *Nature*, *434*(7029), 63–66. Retrieved from http://www.nature.com/articles/nature03365 doi: 10.1038/nature03365

Dai, Z., Keating, E., Bacon, D., Viswanathan, H., Stauffer, P., Jordan, A., & Pawar, R. (2014). Probabilistic evaluation of shallow groundwater resources at a hypothetical carbon sequestration site. *Scientific Reports*, *4*, 1–7. doi: 10.1038/srep04006

De Paula E Silva, F., & Cavaguti, N. (1994). A new stratigraphic and tectonic characterization of the Mesozoic sequence in the city of Bauru - SP. *Geociencias (Sao Paulo)*, *13*(1), 83–99. Retrieved from https://www.scopus.com/

inward/record.uri?eid=2-s2.0-0028603143{\&}partnerID=40{\&}md5=
18f89c8a25aba2729b13d124776f9143

Enemark, T., Peeters, L. J., Mallants, D., & Batelaan, O. (2019). Hydrogeological conceptual model building and testing: A review. *Journal of Hydrology*, *569*, 310–329. doi: 10.1016/j.jhydrol.2018.12.007

Fernandes, A. J., Maldaner, C. H., Negri, F., Rouleau, A., & Wahnfried, I. D. (2016). Aspects of a conceptual groundwater flow model of the Serra Geral basalt aquifer (Sao Paulo, Brazil) from physical and structural geology data. *Hydrogeology Journal*, *24*(5), 1199–1212. doi: 10.1007/s10040-016-1370-6

Fontaine, S., Barot, S., Barré, P., Bdioui, N., Mary, B., & Rumpel, C. (2007). Stability of organic carbon in deep soil layers controlled by fresh carbon supply. *Nature*, *450*(7167), 277–280. doi: 10.1038/nature06275

Foster, S., Hirata, R., Vidal, A., Schmidt, G., & Garduño, H. (2009). The Guarani Aquifer Initiative – Towards Realistic Groundwater Management in a Transboundary Context. *System*(Figure 1), 28.

Freeze, R. A., & Witherspoon, P. A. (1968). Theoretical Analysis of Regional Ground Water Flow: 3. Quantitative Interpretations. *Water Resources Research*, *4*(3), 581–590. doi: 10.1029/WR004i003p00581

Gaillardet, J., Dupré, B., Louvat, P., & Allègre, C. J. (1999, jul). Global silicate weathering and CO2 consumption rates deduced from the chemistry of large rivers. *Chemical Geology*, *159*(1-4), 3–30. Retrieved from https://linkinghub.elsevier.com/retrieve/pii/S0009254199000315 doi: 10.1016/S0009-2541(99)00031-5

Gastmans, D., Chang, H. K., & Hutcheon, I. (2010). Groundwater geochemical evolution in the northern portion of the Guarani Aquifer System (Brazil) and its relationship to diagenetic features. *Applied Geochemistry*, *25*(1), 16–33. Retrieved from http://dx.doi.org/10.1016/j.apgeochem.2009.09.024 doi: 10.1016/j.apgeochem.2009.09.024

Gesicki, A. L. D. (2007). *Diagenetic Evolution of the Pirambóia and Botucatu formations (Guarani Aquifer System) in theSão Paulo state (in Portuguese).* (Unpublished doctoral dissertation). University of São Paulo.

Hansen, B., & Postma, D. (1995). Acidification, buffering, and salt effects in the unsaturated zone of a sandy aquifer, klosterhede, denmark. *Water Resources Re-*

search, *31*(11), 2795–2809.

Herman, J., & Usher, W. (2017, jan). SALib: An open-source python library for sensitivity analysis. *The Journal of Open Source Software*, *2*(9). Retrieved from `https://doi.org/10.21105/joss.00097` doi: 10.21105/joss.00097

Hirata, R., Gesicki, A., Sracek, O., Bertolo, R., Giannini, P. C., & Aravena, R. (2011). Relation between sedimentary framework and hydrogeology in the Guarani Aquifer System in São Paulo state, Brazil. *Journal of South American Earth Sciences*, *31*(4), 444–456. doi: 10.1016/j.jsames.2011.03.006

Jakobsen, R., Kazmierczak, J., Sø, H. U., & Postma, D. (2018). Spatial Variability of Groundwater Arsenic Concentration as Controlled by Hydrogeology: Conceptual Analysis Using 2-D Reactive Transport Modeling. *Water Resources Research*, *54*(12), 10,254–10,269. doi: 10.1029/2018WR023685

Jessen, S., Postma, D., Thorling, L., Müller, S., Leskelä, J., & Engesgaard, P. (2017). Decadal variations in groundwater quality: A legacy from nitrate leaching and denitrification by pyrite in a sandy aquifer. *Water Resources Research*, *53*(1), 184–198. doi: 10.1002/2016WR018995

Kessler, T. J., & Harvey, C. F. (2001). The global flux of carbon dioxide into groundwater. *Geophysical Research Letters*, *28*(2), 279–282. doi: 10.1029/2000GL011505

Li, L., Maher, K., Navarre-Sitchler, A., Druhan, J., Meile, C., Lawrence, C., ... Beisman, J. (2017). Expanding the role of reactive transport models in critical zone processes. *Earth-Science Reviews*, *165*(January 2017), 280–301. doi: 10.1016/j.earscirev.2016.09.001

Li, Y., Wang, Y. G., Houghton, R. A., & Tang, L. S. (2015). Hidden carbon sink beneath desert. *Geophysical Research Letters*, *42*(14), 5880–5887. doi: 10.1002/2015GL064222

Maher, K., & Chamberlain, C. P. (2014). Hydrologic regulation of chemical weathering and the geologic carbon cycle. *Science*, *343*(6178), 1502–1504. doi: 10.1126/science.1250770

McCallum, J. L., Cook, P. G., Berhane, D., Rumpf, C., & McMahon, G. A. (2012). Quantifying groundwater flows to streams using differential flow gaugings and water chemistry. *Journal of Hydrology*, *416-417*, 118–132. Retrieved from `http://dx.doi.org/10.1016/j.jhydrol.2011.11.040` doi:

10.1016/j.jhydrol.2011.11.040

Meng, S. X., & Maynard, J. B. (2001). Use of statistical analysis to formulate conceptual models of geochemical behavior: Water chemical data from the Botucatu aquifer in São Paulo state, Brazil. *Journal of Hydrology*, *250*(1-4), 78–97. doi: 10.1016/S0022-1694(01)00423-1

Oelkers, E. H., Declercq, J., Saldi, G. D., Gislason, S. R., & Schott, J. (2018). Olivine dissolution rates: A critical review. *Chemical Geology*, *500*(October), 1–19. doi: 10.1016/j.chemgeo.2018.10.008

Parkhurst, D. L., Kipp, K. L., & Charlton, S. R. (2010). *PHAST Version 2 - A program for simulating groundwater flow, solute transport, and multicomponent geochemical reactions* (Vol. 6–A35; Tech. Rep.). U.S. Geological Survey Techniques and Methods 6–A35. Retrieved from `http://pubs.usgs.gov/tm/06A35/`

Plischke, E., Borgonovo, E., & Smith, C. L. (2013). Global sensitivity measures from given data. *European Journal of Operational Research*, *226*(3), 536–550. Retrieved from `http://dx.doi.org/10.1016/j.ejor.2012.11.047` doi: 10.1016/j.ejor.2012.11.047

Pogge von Strandmann, P. A., Burton, K. W., Snæbjörnsdóttir, S. O., Sigfússon, B., Aradóttir, E. S., Gunnarsson, I., ... Gislason, S. R. (2019). Rapid CO 2 mineralisation into calcite at the CarbFix storage site quantified using calcium isotopes. *Nature Communications*, *10*(1), 1–7. doi: 10.1038/s41467-019-10003-8

Postma, D., & Jakobsen, R. (1996). Redox zonation: Equilibrium constraints on the Fe(III)/SO4-reduction interface. *Geochimica et Cosmochimica Acta*, *60*(17), 3169–3175.

Rebouças, A. C. (1976). *Recursos Hídricos Subterrâneos da Bacia do Paraná - Analise de Pre-Viabilidade* (Unpublished doctoral dissertation). Université de Strasbourg.

Rebouças, A. C. (1994). Sistema Aqüífero Botucatu no Brasil. In *Viii congresso brasileiro de águas subterrâneas* (pp. 500–509).

Rodríguez-Zorro, P. A., Ledru, M.-P., Bard, E., Aquino-Alfonso, O., Camejo, A., Daniau, A.-L., ... Thouveny, N. (2020). Shut down of the South American summer monsoon during the penultimate glacial. *Scientific Reports*, *10*(1), 1–11. doi: 10.1038/s41598-020-62888-x

Sánchez-Cañete, E. P., Barron-Gafford, G. A., & Chorover, J. (2018). A considerable fraction of soil-respired CO2 is not emitted directly to the atmosphere. *Scientific Reports*, *8*(1), 2–11. doi: 10.1038/s41598-018-29803-x

Silva, R. B. G. (1983). *Hydrogeochemical and isotopic study of ground-water of the Botucatu Aquifer, in São Paulo state (in Portuguese).* (Unpublished doctoral dissertation). University of São Paulo.

Soler i Gil, A., & Bonotto, D. M. (2014). Hydrochemical and stable isotopes (H, O, S) signatures in deep groundwaters of Paraná basin, Brazil. *Environmental Earth Sciences*, *73*(1), 95–113. doi: 10.1007/s12665-014-3397-0

Sracek, O., & Hirata, R. (2002, dec). Geochemical and stable isotopic evolution of the Guarani Aquifer System in the state of São Paulo, Brazil. *Hydrogeology Journal*, *10*(6), 643–655. Retrieved from `http://link.springer.com/10.1007/s10040-002-0222-8` doi: 10.1007/s10040-002-0222-8

Steefel, C. I., DePaolo, D. J., & Lichtner, P. C. (2005, dec). Reactive transport modeling: An essential tool and a new research approach for the Earth sciences. *Earth and Planetary Science Letters*, *240*(3-4), 539–558. Retrieved from `https://linkinghub.elsevier.com/retrieve/pii/S0012821X05005984` doi: 10.1016/j.epsl.2005.09.017

Steffen, W., Crutzen, J., & McNeill, J. R. (2007). The Anthropocene: are humans now overwhelming the great forces of Nature? *Ambio*, *36*(8), 614–21. Retrieved from `http://www.ncbi.nlm.nih.gov/pubmed/18240674` doi: 10.1579/0044-7447(2007)36[614:taahno]2.0.co;2

Vilhelmsen, T. N., Maher, K., Da Silva, C., Hermans, T., Grujic, O., Park, J., & Yang, G. (2018a). The earth resources challenge. In *Quantifying uncertainty in subsurface systems* (p. 1-27). American Geophysical Union (AGU). Retrieved from `https://agupubs.onlinelibrary.wiley.com/doi/abs/10.1002/9781119325888.ch1` doi: 10.1002/9781119325888.ch1

Vilhelmsen, T. N., Maher, K., Da Silva, C., Hermans, T., Grujic, O., Park, J., & Yang, G. (2018b). Quantifying uncertainty in subsurface systems. In *Quantifying uncertainty in subsurface systems* (p. 217-262). American Geophysical Union (AGU). Retrieved from `https://agupubs.onlinelibrary.wiley.com/doi/abs/10.1002/9781119325888.ch8` doi: 10.1002/9781119325888.ch8

Walraevens, K., Cardenal-Escarcena, J., & Van Camp, M. (2007). Reac-

tion transport modelling of a freshening aquifer (Tertiary Ledo-Paniselian Aquifer, Flanders-Belgium). *Applied Geochemistry*, *22*(2), 289–305. doi: 10.1016/j.apgeochem.2006.09.006

Wendland, E., Barreto, C., & Gomes, L. H. (2007). Water balance in the Guarani Aquifer outcrop zone based on hydrogeologic monitoring. *Journal of Hydrology*, *342*(3-4), 261–269. doi: 10.1016/j.jhydrol.2007.05.033

White, A. F., & Brantley, S. L. (2003). The effect of time on the weathering of silicate minerals: Why do weathering rates differ in the laboratory and field? *Chemical Geology*, *202*(3-4), 479–506. doi: 10.1016/j.chemgeo.2003.03.001

Zhang, S., & Planavsky, N. J. (2020). Revisiting groundwater carbon fluxes to the ocean with implications for the carbon cycle. *Geology*, *XX*(Xx), 1–5. doi: 10.1130/G46408.1/4870418/g46408.pdf

Zhong, J., Li, S. L., Tao, F., Yue, F., & Liu, C. Q. (2017). Sensitivity of chemical weathering and dissolved carbon dynamics to hydrological conditions in a typical karst river. *Scientific Reports*, *7*(October 2016), 1–9. doi: 10.1038/srep42944

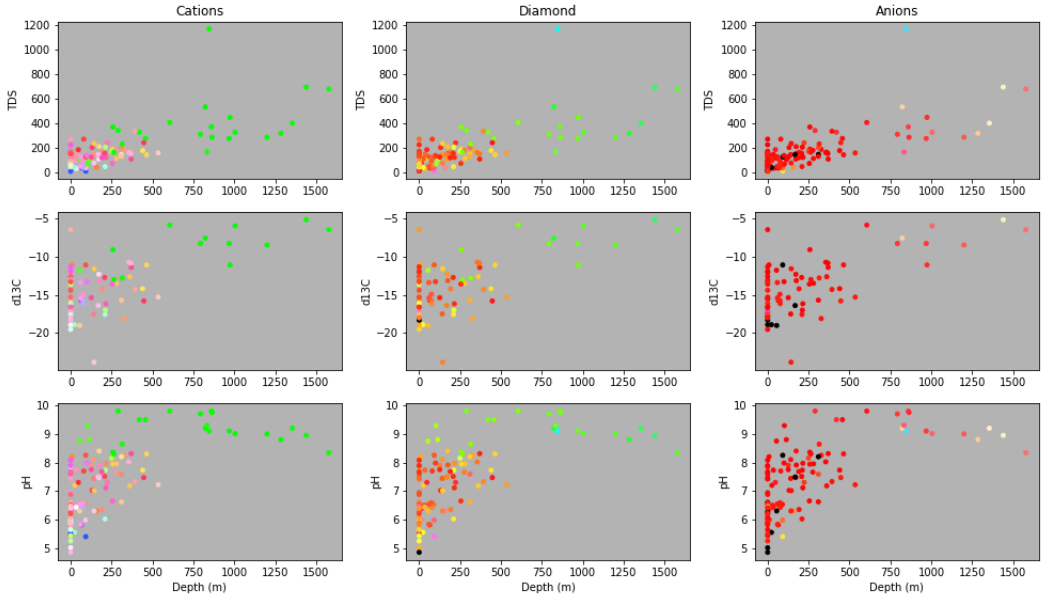

Figure A1. Variations in water quality parameters over depth with a color depicting a water type. Black points pertain to samples whose water type was not determined (Gastmans et al., 2010)

Appendix A Variations in selected water quality parameters over depth

Appendix B Sensitivity indexes and confidence intervals

Appendix C Groundwater well location

Table B1. Sensitivity indexes for outputs and corresponding parameters, Part 1/2

	Distance, km	K	Mg	heads	Ca	pH	alk	C	Na	Si
	50	1.11e-02	6.41e-02	8.16e-01	4.49e-02	2.92e-01	7.02e-02	2.45e-01	4.94e-02	6.93e-02
C recharge	150	1.32e-02	5.04e-02	8.16e-01	5.60e-02	2.26e-01	8.25e-02	1.86e-01	5.96e-02	8.39e-02
	250	1.24e-02	2.84e-02	8.15e-01	4.44e-02	1.67e-01	6.34e-02	1.34e-01	4.40e-02	6.50e-02
	50	5.45e-03	1.50e-03	6.72e-03	4.18e-03	7.69e-04	3.90e-03	4.25e-03	4.06e-03	3.83e-03
$K_{calcite}$	150	5.88e-03	8.12e-04	6.71e-03	4.67e-03	9.02e-04	4.60e-03	2.14e-03	4.57e-03	4.56e-03
	250	5.57e-03	3.64e-04	6.61e-03	5.24e-03	8.43e-04	5.21e-03	2.44e-03	5.18e-03	5.13e-03
	50	3.85e-03	5.99e-03	5.08e-03	2.89e-03	2.51e-02	2.80e-03	2.11e-02	3.14e-03	2.70e-03
Kx	150	3.86e-03	4.93e-03	5.07e-03	2.46e-03	3.02e-02	3.40e-03	2.39e-02	2.73e-03	3.47e-03
	250	4.03e-03	4.21e-03	5.00e-03	2.25e-03	2.88e-02	3.44e-03	2.38e-02	2.44e-03	3.62e-03
	50	5.01e-03	3.71e-03	1.73e-02	9.82e-03	8.04e-03	9.63e-03	6.69e-03	9.70e-03	9.54e-03
Mg_{ratio}	150	4.24e-03	4.81e-03	1.73e-02	9.60e-03	8.69e-03	9.08e-03	1.28e-02	9.07e-03	9.01e-03
	250	3.55e-03	7.54e-03	1.72e-02	9.08e-03	6.63e-03	8.41e-03	1.04e-02	8.27e-03	8.38e-03
	50	4.49e-03	5.10e-03	5.51e-03	6.12e-03	2.86e-03	5.46e-03	6.76e-04	6.11e-03	5.58e-03
Porosity	150	4.54e-03	3.79e-03	5.51e-03	5.71e-03	5.30e-03	4.96e-03	2.80e-03	5.63e-03	4.92e-03
	250	4.61e-03	3.25e-03	5.46e-03	5.11e-03	4.78e-03	4.53e-03	2.95e-03	5.10e-03	4.46e-03

Table B2. Sensitivity indexes for outputs and corresponding parameters, Part 2/2

	Distance, km	K	Mg	heads	Ca	pH	alk	C	Na	Si
	50	1.75e-02	3.82e-04	3.12e-03	4.76e-03	1.73e-02	4.68e-03	1.07e-02	4.86e-03	4.63e-03
$r_{K-feldspar}$	150	3.06e-02	2.73e-04	3.12e-03	6.65e-03	3.05e-02	6.36e-03	7.63e-03	6.58e-03	6.24e-03
	250	4.46e-02	7.36e-04	3.09e-03	7.69e-03	3.47e-02	7.49e-03	5.78e-03	7.64e-03	7.32e-03
	50	5.18e-03	1.93e-01	4.44e-04	6.20e-03	1.20e-01	5.31e-03	1.10e-01	5.96e-03	5.54e-03
$r_{Olivine}$	150	4.73e-03	2.55e-01	4.44e-04	3.61e-03	1.55e-01	3.14e-03	9.71e-02	3.54e-03	3.31e-03
	250	4.56e-03	2.75e-01	4.37e-04	3.26e-03	1.68e-01	2.23e-03	1.26e-01	3.19e-03	2.48e-03
	50	5.13e-03	3.68e-03	6.13e-03	7.82e-02	3.98e-01	8.91e-02	2.27e-01	8.34e-02	8.86e-02
$r_{Plagioclase}$	150	4.74e-03	4.69e-03	6.13e-03	1.45e-01	3.56e-01	1.63e-01	3.93e-01	1.52e-01	1.68e-01
	250	4.13e-03	4.83e-03	6.10e-03	1.87e-01	3.52e-01	2.09e-01	4.14e-01	1.94e-01	2.15e-01
	50	3.99e-03	6.39e-03	2.40e-04	3.13e-03	1.50e-03	2.72e-03	2.16e-03	3.15e-03	2.79e-03
SI_{illite}	150	3.39e-03	7.56e-03	2.41e-04	2.48e-03	3.93e-03	2.36e-03	4.00e-03	2.44e-03	2.40e-03
	250	2.93e-03	7.55e-03	2.47e-04	1.60e-03	4.07e-03	1.65e-03	3.73e-03	1.52e-03	1.65e-03
	50	5.84e-03	1.58e-03	1.24e-02	1.43e-02	9.07e-03	1.46e-02	5.49e-03	1.45e-02	1.44e-02
SI_{K-mica}	150	6.08e-03	1.67e-03	1.24e-02	1.75e-02	1.14e-02	1.66e-02	6.85e-03	1.77e-02	1.64e-02
	250	5.88e-03	2.03e-03	1.25e-02	1.75e-02	1.30e-02	1.64e-02	9.71e-03	1.75e-02	1.64e-02
	50	5.05e-03	4.44e-03	4.87e-03	3.42e-03	2.03e-03	2.54e-03	5.17e-03	3.41e-03	2.53e-03
Soil pH	150	4.51e-03	4.69e-03	4.88e-03	4.94e-03	2.36e-03	4.03e-03	4.91e-03	4.87e-03	4.03e-03
	250	4.33e-03	4.54e-03	4.88e-03	5.46e-03	4.70e-03	4.62e-03	7.20e-03	5.40e-03	4.60e-03

Table B3. Confidence intervals for outputs and corresponding parameters, Part 1/2

	Distance, km	Mg	K	heads	C	alk	Si	Ca	Na	pH
	50	3.62e-02	2.01e-02	2.78e-02	8.79e-02	3.08e-02	1.69e-02	1.56e-02	2.01e-02	4.77e-02
C recharge	150	3.29e-02	1.68e-02	1.87e-02	4.07e-02	3.17e-02	2.04e-02	3.54e-02	2.43e-02	6.06e-02
	250	3.00e-02	1.22e-02	2.19e-02	2.96e-02	1.84e-02	2.99e-02	1.84e-02	2.74e-02	3.28e-02
	50	8.29e-03	5.05e-03	8.57e-03	8.04e-03	5.64e-03	5.17e-03	9.69e-03	5.94e-03	1.22e-02
$K_{calcite}$	150	6.31e-03	6.84e-03	5.76e-03	1.36e-02	7.62e-03	1.27e-02	1.07e-02	8.49e-03	5.79e-03
	250	6.74e-03	4.99e-03	1.37e-02	6.23e-03	1.17e-02	1.23e-02	9.04e-03	9.07e-03	7.67e-03
	50	6.66e-03	1.16e-02	1.04e-02	1.90e-02	6.61e-03	1.04e-02	7.01e-03	6.77e-03	1.62e-02
Kx	150	6.18e-03	6.38e-03	1.18e-02	2.04e-02	1.45e-02	1.02e-02	7.31e-03	1.62e-02	1.88e-02
	250	1.11e-02	7.60e-03	4.58e-03	2.01e-02	6.68e-03	7.05e-03	7.06e-03	1.16e-02	1.99e-02
	50	5.78e-03	9.16e-03	2.50e-02	1.25e-02	1.21e-02	9.13e-03	6.00e-03	1.26e-02	1.15e-02
Mg_{ratio}	150	8.95e-03	6.20e-03	1.39e-02	1.37e-02	1.37e-02	1.35e-02	9.38e-03	8.87e-03	1.58e-02
	250	1.21e-02	5.59e-03	7.98e-03	1.61e-02	9.41e-03	9.87e-03	1.33e-02	9.83e-03	1.33e-02
	50	1.06e-02	5.86e-03	8.50e-03	7.39e-03	7.24e-03	8.36e-03	8.26e-03	7.38e-03	3.84e-03
Porosity	150	1.18e-02	8.76e-03	7.19e-03	1.05e-02	3.29e-03	1.12e-02	1.30e-02	1.05e-02	7.39e-03
	250	9.50e-03	6.99e-03	1.13e-02	8.19e-03	8.47e-03	8.69e-03	7.56e-03	1.29e-02	6.39e-03

Table B4. Confidence intervals for outputs and corresponding parameters, Part 2/2

	Distance, km	Mg	K	heads	C	alk	Si	Ca	Na	pH
	50	8.80e-03	8.70e-02	1.00e-02	1.25e-02	6.94e-03	9.47e-03	7.74e-03	3.60e-03	1.73e-02
$r_{K-feldspar}$	150	8.38e-03	1.04e-01	1.06e-02	1.46e-02	1.50e-02	1.39e-02	8.50e-03	8.14e-03	1.56e-02
	250	5.81e-03	6.69e-02	4.96e-03	1.48e-02	1.10e-02	1.13e-02	1.24e-02	9.59e-03	1.90e-02
	50	8.41e-02	4.34e-03	7.43e-03	2.71e-02	9.37e-03	6.78e-03	6.22e-03	1.01e-02	4.81e-02
$r_{Olivine}$	150	6.84e-02	4.62e-03	3.89e-03	3.56e-02	1.15e-02	1.70e-02	6.39e-03	5.30e-03	4.08e-02
	250	8.58e-02	6.17e-03	5.27e-03	3.05e-02	1.12e-02	5.47e-03	7.86e-03	7.69e-03	2.43e-02
	50	6.30e-03	9.25e-03	9.75e-03	6.47e-02	3.57e-02	3.54e-02	4.27e-02	9.21e-02	8.59e-02
$r_{Plagioclase}$	150	9.33e-03	9.17e-03	1.45e-02	4.59e-02	4.42e-02	7.53e-02	3.16e-02	5.41e-02	5.09e-02
	250	8.66e-03	1.64e-02	8.03e-03	5.05e-02	3.24e-02	4.44e-02	3.68e-02	4.03e-02	5.18e-02
	50	1.06e-02	1.04e-02	1.02e-02	3.68e-03	7.51e-03	7.66e-03	7.09e-03	1.08e-02	7.87e-03
SI_{illite}	150	7.87e-03	8.48e-03	7.96e-03	8.38e-03	5.23e-03	5.80e-03	8.26e-03	7.15e-03	1.13e-02
	250	9.72e-03	8.00e-03	4.62e-03	1.44e-02	7.30e-03	8.41e-03	7.69e-03	9.16e-03	7.30e-03
	50	7.59e-03	7.89e-03	1.24e-02	7.94e-03	1.09e-02	1.07e-02	1.11e-02	1.49e-02	7.94e-03
SI_{K-mica}	150	5.33e-03	5.55e-03	1.33e-02	8.96e-03	1.66e-02	1.96e-02	1.82e-02	1.13e-02	1.38e-02
	250	8.91e-03	1.07e-02	1.54e-02	1.58e-02	3.00e-02	1.80e-02	2.11e-02	1.63e-02	1.13e-02
	50	4.50e-03	1.17e-02	1.23e-02	6.24e-03	7.77e-03	6.63e-03	8.83e-03	9.75e-03	7.07e-03
Soil pH	150	1.57e-02	6.42e-03	1.32e-02	1.14e-02	4.90e-03	8.50e-03	1.13e-02	6.19e-03	5.58e-03
	250	9.16e-03	5.18e-03	9.74e-03	1.42e-02	8.60e-03	7.62e-03	1.05e-02	3.59e-03	8.72e-03

Table C1. Groundwater sampling wells with the interpreted distances (km) along the groundwater flow path from the basin margin

Well ID	Location	Latitude (S)	Longitude (W)	Flow path symbol	Distance (km)
SP104	Itirapina	-22.30	-47.80	□	0.0
SP095	São Carlos	-22.07	47.90	□	30.04
SP083	Ibaté	-21.97	-47.98	□	45.63
SP080	Araraquara	-21.78	-48.15	□	71.25
SP065	Matão	-21.60	-48.37	□	99.9
SP061	Itáopolis	-21.58	-48.80	□	146.0
SP044	Novo Horizonte	-21.47	-49.23	□	191.6
SP149	Botucatú	-22.92	-48.45	▽	46.6
SP135	Macatuba	-22.47	-48.77	▽	108.1
SP117	Pederneiras	-22.35	-48.77	▽	118.5
SP111	Bauru	-22.17	-49.03	▽	154.6
SP059	Lins	-21.67	-49.77	▽	245.6
SP902	Araçatuba	-21.17	-50.40	▽	332.3
SP160	Sarutaiá	-23.27	-49.48	△	8.2
SP105	Paraguaçu Pta	-22.42	-50.60	△	98.3
SP087	Pres. Prudente	-22.11	-51.42	△	251.2
PEP	Pres. Epitácio	-21.76	-52.10	△	333.2
SP085	Descalvado	-21.87	-47.63	○	0.0
SP049	Guatapará	-21.50	-48.03	○	59.1
SP900	Guariba	-21.35	-48.22	○	84.2
SP025	Jaboticabal	-21.25	-48.30	○	98.0
SP023	Catanduva	-21.12	-48.97	○	168.4